Superoxide Dismutases maintain niche homeostasis in stem cell populations

Olivia Majhi[1], Aishwarya Chhatre[1,2], Tanvi Chaudhary[1] and Devanjan Sinha[1#]

[1]Department of Zoology, Institute of Science, Banaras Hindu University, Varanasi, Uttar Pradesh, India

[2]Present address: Biological Research Centre, Institute of Genetics, Eötvös Loránd Research Network (ELKH), Szeged, Hungary

[#]To whom correspondence should be addressed:

Address for correspondence:
Dr. Devanjan Sinha,
Department of Zoology,
Institute of Science,
Banaras Hindu University,
Varanasi – 221005,
Uttar Pradesh, India
India
Email: devanjan@bhu.ac.in

Abstract

Reactive oxygen species (ROS), predominantly derived from mitochondrial respiratory complexes, have emerged as key molecules influencing cell fate decisions like maintenance and differentiation. These redox-dependent events are mainly considered to be cell intrinsic in nature, on the contrary our observations indicate involvement of these oxygen-derived entities as intercellular communicating agents. In *Drosophila* male germline, Germline Stem Cells (GSCs) and neighbouring Cyst Stem Cells (CySCs) maintain differential redox thresholds where CySC have higher redox-state compared to the adjacent GSCs. Disruption of the redox equilibrium between the two adjoining stem cell populations by depleting Superoxide Dismutases (SODs) especially Sod1 results in deregulated niche architecture and loss of GSCs, which was mainly attributed to loss of contact-based receptions and uncontrolled CySC proliferation due to ROS-mediated activation of self-renewing signals. Our observations hint towards the crucial role of differential redox states where CySCs containing higher ROS function not only as a source of their own maintenance cues but also serve as non-autonomous redox moderators of GSCs. Our findings underscore the complexity of niche homeostasis and predicate the importance of intercellular redox communication in understanding stem cell microenvironments.

52 **Introduction**

53 Studies from the past few decades have shown the apparent role of ROS in influencing
54 various biological processes[1-3]. ROS are usually produced in specific cellular
55 compartments close to their target molecules to regulate important signaling
56 pathways.[4]. Mitochondria, a major source of oxidant species[5,6], localize dynamically
57 towards nucleus, effecting oxidation induced reshaping of gene expression profiles[7].
58 Localized ROS production are contributed by NADH oxidases distributed across
59 different cellular regions[8]. Intracellular hydrogen peroxide gradients, maintained by
60 thioredoxin system, allow intercompartmental exchanges among endoplasmic
61 reticulum (ER), mitochondria and peroxisomes[9-11].

62 The process of redox relays is conserved and plays a fundamental role in self-renewal
63 and differentiation of stem cell populations[12]. Stem cells whether embryonic or adult
64 generally maintain a low redox profile, barring few exceptions and are characterized
65 by subdued mitochondrial respiration[13-17]. Levels of ROS are tightly regulated and
66 elevated amounts promote early differentiation and atypical stem cell behaviour[18].
67 However, leading evidences suggest that many transcription factors require oxidative
68 environment for the maintenance of pluripotent states. For instance, physiological
69 ROS levels play a crucial role in genome maintenance of embryonic stem cells[13].
70 Multipotent hematopoietic progenitors, intestinal stem cells [19] and neural stem cells
71 require relatively high baseline redox for their maintenance[14,16,20]. Suppression of Nox
72 system or mitochondrial ROS compromises the maintenance of these self-renewing
73 populations and promote their differentiation or death[18]. These evidences point
74 towards the essentiality of a well-tuned redox state for balancing the pluripotent and
75 differentiated states. However, how stem cells regulate their redox potential by
76 possessing a restrained oxidant system is not very clear.

77 We addressed this fundamental question in two-stem cell population-based niche
78 architecture in *Drosophila* testis. The testicular stem cell niche is composed of a
79 central cluster of somatic cells called the hub which contacts eight to eleven GSCs
80 arranged in a round array[21,22]. A pair of cyst stem cells (CySCs) enclose each GSC
81 and make their independent connections with the hub and GSCs via adherens
82 junctions[23-28]The hub cells secrete self-renewal factors essential for both GSCs and
83 CySCs maintenance involving signalling cascades like Jak-Stat signalling[29,30], BMP

84 (Bone Morphogenetic Signalling)[31], Hedgehog signalling[32]. The hub and CySCs
85 produce BMPs which repress GSC differentiation by suppressing transcription of bag-
86 of-marbles (Bam)[31,33]. Asymmetric division of both GSC and CySC is essential for
87 proper cyst formation[3435]. A developing cyst contains a dividing and differentiating
88 gonialblast encircled by cyst cells that provide nourishment to developing
89 spermatids[36,37]. However, the maintenance of GSCs in the spatially controlled
90 microenvironment is still not very clear.

91 We found the existence of a balanced differential redox state between GSC and CySC
92 to be essential for niche homeostasis. CySCs by virtue of their higher redox threshold
93 and more clustered mitochondria generated an intercellular redox state that affected
94 the physiological ROS levels in GSCs. Alterations in CySC redox state affected the
95 self-renewal and differentiation propensities of the GSCs. Intercellular redox
96 imbalance disrupts niche homeostasis by inducing premature differentiation of
97 germline stem cells (GSCs) and aberrant proliferation of cyst stem cells (CySCs),
98 driven by activation of pro-proliferative signaling pathways and attenuation of cell–cell
99 contact–mediated communication. Our results indicated a sophisticated interplay
100 between these two stem cell populations where a higher redox state in CySCs not only
101 supports their self-renewing processes but also non-autonomously promotes the
102 maintenance of GSCs.

103

104 **Results**

105 **CySCs maintain higher differential ROS in comparison to adjacent GSCs**

106 The apical region of the *Drosophila* testis incorporates a cluster of differentiated cells,
107 the hub which is surrounded by GSCs in a rosette arrangement with each GSC being
108 enclosed by two CySCs (Fig. 1A). Immunostaining the ATP5A subunit of mitochondrial
109 ATPase and marking cell boundary by discs-large (Dlg) indicated different
110 mitochondrial distribution among these two stem cell populations. In wild type adult
111 testis, we observed sparsely populated mitochondria in Vasa^{+} GSCs as compared to
112 their dense distribution in CySCs (Fig. 1B#, C, D, and S1B-B”). The number of
113 mitochondria per cell was higher in CySC (Fig. 1F). The ATP5A labelling overlapped
114 with *TFAM-GFP*, a mitochondrial transcription factor[38] that labelled the mitochondria,

115 further confirming the patterning observed between these two stem cell populations
116 (Fig. S1A). Since mitochondria are known to be one of the major producers of ROS in
117 cells, we tested for the relative redox profiles in these two stem cell populations.
118 Mitochondrial dispersion pattern in GSCs and CySCs, corresponded with the intensity
119 variance of the ROS reporter line *gstD1-GFP*[39] among the different cell populations at
120 the niche. CySCs (outlined by a dotted boundary) exhibited distinctly higher *gstD1*
121 reporter intensity than the neighbouring GSC (shown with yellow arrowhead) (Fig. 1K
122 and S1C'''). Quantification of this intensity difference indicated that CySCs exhibited a
123 higher baseline level of ROS compared to GSCs (Fig.1Q). The hub zone (denoted by
124 asterisk) also presented higher *gstD1-GFP* intensity when compared to the
125 surrounding germline (Fig. 1K and S1C''').

126 Given the ability of free-radicals to diffuse, we hypothesized that the somatically
127 derived cells in the niche, by virtue to their higher ROS state might be maintaining the
128 redox environment of their surroundings. In this study, we evaluated the redox
129 interplay between the two stem cell population in the niche. To test the role of CySC
130 in influencing GSC redox state, we asked if disrupting the superoxide dismutases in
131 CySCs would influence the redox state of GSCs. To deplete SOD1, we used *Tj-Gal4*[40]
132 driver (*Tj>Sod1i*) that expresses majorly in CySCs and early differentiating cyst cells
133 (CCs) with minor levels of expression in the hub. Depletion of SOD1 majorly in CySCs
134 resulted in a net increase in *gstD1*-GFP intensity in the niche zone (Fig. 1P, R and
135 S1E), and an overall rise in superoxide levels, confirmed through DHE fluorescence
136 analysis (Fig.S1F). Increased *gstD1* labelling due to SOD1 depletion in CySC
137 (denoted by dotted area) (Fig. 1P, S1D''') adjacent to Vasa+ GSC (shown with yellow
138 arrow), resulted in concomitant increase in *gstD1* intensity at the Vasa+ GSC (Fig. 1P,
139 S1D'''). This indicates that the elevated redox state in CySCs led to a corresponding
140 increase in ROS levels in adjacent GSCs (Fig. 1R) suggesting a potential redox
141 crosstalk between these stem cell populations, where the redox state of CySCs might
142 be influencing the oxidative status of neighbouring GSCs. This crosstalk was further
143 validated by subsequent phenotypic analysis.

144

145 **Balanced CySC redox profile is crucial for its proliferation and GSC**
146 **maintenance**

147 Alongside the differential redox profile, we observed that elevated ROS levels in
148 *Tj>Sod1i* had a striking effect on the increase of DAPI$^+$ nuclei at the testis tip (Fig.
149 2A''). This overcrowding was attributed to both an increase in the number of Tj$^+$ CySCs
150 and early differentiating CCs, as well as their positional shift (Fig. 2A', B', and E). To
151 further validate these findings, we used an alternative driver line, *C-587-Gal4*, which
152 specifically drives expression in CySCs and CCs. This also resulted in an increase in
153 the total number of Tj$^+$ cells (Fig. S1H', and M) although to a lesser extent than *Tj-*
154 *Gal4*, suggesting that signals from the hub may also partially influence CySC
155 proliferation. Given the stronger phenotypic effect observed with *Tj-Gal4*, we
156 proceeded with this driver line for subsequent experiments.

157 The enhancement in the number of CySCs was also reflected by ~2-fold change in
158 Zfh1$^+$ cells (Fig. 2F, S2R(I)-S(I)). However, Vasa$^+$ cells flanking the hub (GSCs)
159 showed a substantial reduction in number (Fig. 2C''-D'' and G). This decline was
160 further validated by western blot analysis, which revealed lower overall detectable
161 levels of Vasa protein, indicating a potential impact of the altered redox state on
162 germline maintenance (Fig. S2N). Since, Tj shows a minor expression in hub cells, we
163 validated our phenotypic data using *C-587-Gal4* that is specific for CySCs and CCs.
164 Similar to *Tj>Sod1*, *C-587-Gal4>Sod1i* also showed a reduction in the number of
165 neighbouring GSCs (Fig.S1N). The observations were further verified using *Sod1i*
166 localized in different chromosome to avoid any chromosome or balancer-based
167 biasness and a similar result was obtained where alterations in CySC ROS affected
168 GSC number (Fig. S1I-L and O-P). However, the phenotypic effect of higher ROS was
169 limited to its origin in CySCs only because ablation of GSC redox status did not cause
170 any marked change in niche composition. *Nos-Gal4* driven knock-down of Sod1 in
171 GSCs did not result in significant change in CySC number (Fig. S2A', B' and E) but
172 effected a considerable reduction on Vasa$^+$ cells (Fig. S2C', D' and F), aligning with
173 previous observations[17]. Although Sod1 is the predominant enzyme which also
174 localizes in the intermembrane space of mitochondria, we observed a similar result
175 upon depleting the matrix localized Sod2 in both GSCs and CySCs (Fig. S2G-M),
176 indicating the involvement of mitochondrial ROS for the observed cellular phenotypes.

177 To confirm the active proliferation of cells and rule out the possibility of arrested
178 growth, we utilized fly-Fluorescent Ubiquitination-based Cell Cycle Indicator (FUCCI)
179 system[41] which comprises of two reporter constructs marking G1/S transition (green),

180 S (red) and G2/early mitosis (yellow) (Fig. 2H). Testes from *Tj>Sod1i* exhibited an
181 approximately two-fold increase in cell number across all stages of the cell cycle (Fig.
182 S2O). However, the percentage of cells in each phase remained unchanged (Fig 2I),
183 indicating that the observed increase in different phases is a consequence of more
184 cells entering proliferation rather than alterations in the duration of different cell-cycle
185 stages. The enhanced number of dividing cells was contributed mainly by progressive
186 division of CySCs, showing >2-fold difference in the accumulation of Zfh1^{+} nuclei in S
187 and G2/M phases (Fig. 2J, S2RV-VII and SV-VII). The number of Zfh1 labelled cells
188 in G1/S transition was also substantially more (Fig. S2RIII and SIII), indicating
189 dysregulated redox ensued an increased mitotic index of CySCs. The enhanced
190 mitotic activity of these proliferating niche cells is further supported by increased
191 phospho-histone H3 (PH3) incorporation, indicating a higher mitotic frequency
192 compared to the control (Fig. 2K, S2T-U), along with elevated cyclin D expression (Fig.
193 S2Q). Downregulation of Sod1 in GSCs through *Nos-Gal4* demonstrated no significant
194 change in G1/S, S and G2/M phase numbers, confirming our previous observation
195 that altering ROS levels in GSCs does not have any non-autonomous effect on CySCs
196 numbers (Fig. S2P).

197

198 **CySC induced ROS couples precocious differentiation of stem cell lineages**

199 Since in *Tj>Sod1i* testes, the increased number of Tj^{+} cells, marking CySCs and early
200 differentiating cells, exceeded the number of CySC-specific Zfh1^{+} cells (Fig. 2J and
201 S2O), we checked for parallel enhancement of cellular differentiation using the
202 corresponding marker, *Eya* (Eyes absent).

203 We found that Eya^{+} cells clustered towards the hub, along with a significant increase
204 in their number in Sod1 depleted CySCs (Fig. 3A, B and D). This increased number of
205 Eya^{+} cells does not suggest that these differentiating cells are proliferative. Instead,
206 we propose that the knockdown of Sod1 may alter the timing or regulation of cyst cell
207 differentiation, leading to an accumulation of Eya^{+} cells near the niche. The supposed
208 premature expression of Eya resulted in a population of differentiating cyst precursor
209 cells co-expressing Eya-Zfh1 (Fig. 3A'', B'' and D). This population was found to be
210 deviating from the normal partitioning of wild-type representative populations (Fig. 3C).

211 In contrast, depletion of *Sod1i* in the germline lineage using *Nos-Gal4* did not result in
212 a similar phenotypic arrangement (Fig. S3A-D). These findings suggest that alterations
213 in the redox state of GSCs can impact their numbers, even when the changes are
214 induced non-autonomously through CySCs[17].

215 Together with reduction in Vasa^{+} GSCs shown earlier (Fig. 2G), we also detected
216 gonialblast expressing the differentiation-promoting factor Bam, to be much closer to
217 hub in *Tj>Sod1i* testes (Fig. 3E'' and F''). The mean distance between the hub and
218 Bam^{+} cells was found to be shortened by ~7 microns (Fig 3G). The relative
219 advancement of spermatogonial differentiation towards the hub was also ascertained
220 by tracking the transformation of GSC-specific spectrosome into branched fusomes
221 connecting the multi-cell gonialblast (Fig. 1A). The branching fusomes were found
222 more proximal to hub than controls (Fig. 3H, I'' and J''), along with parallel reduction
223 in number of spectrosomes, implying a decline in early-stage germ cells (Fig. S3F).
224 This loss could possibly be attributed to loss of intercellular contacts, particularly with
225 hub cells (Fig. 3K# and L#). The observation corroborated with decreased expression
226 pattern of E-cadherin flanking the hub and GSCs, in *Tj>Sod1i* (Fig. 3M-O) and could
227 be one of the reasons for GSCs dissociation and differentiation (Fig. 3L#),
228 Disengagement of GSCs from the hub caused reduction in Socs36E and Ptp61F
229 transcripts which subsequently alter Stat expression, a key driver of E-cadherin
230 expression (Fig. 3P and Q). These results suggest that disruption of intercellular redox
231 gradient affected the premature differentiation of stem cells in the niche.

232

233 **Disrupted niche architecture compromises GSC-CySC communication**

234 GSCs and CySCs intercommunicate through several factors such as EGFR, PI3K/Tor,
235 Notch[42] to support CySC maintenance[43]. EGF ligands secreted by spermatogonia
236 maintain differences in cell polarity and segregates self-renewing from differentiating
237 populations[44]. *Tj>Sod1i* cells showed lower levels of cell-polarity marker Dlg (Fig. 4A",
238 B" and E), that expanded more into the differentiated zone (Fig. S4A), indicating loss
239 of cell polarity and aligning with the overtly proliferative nature of these cells. Along
240 with Dlg, a net reduction in pErk levels was observed across sections in *Sod1i* testis
241 (Fig. 4C', D' and F). This reduction in overall Erk levels may be attributed to the loss
242 of cell contact and altered GSC-CySC balance in *Sod1i* testis. The proliferation of cyst

243 cells correlated with increased levels of self-renewal inducers, including the elevated
244 expression of Hedgehog (Hh) pathway components[32], in *Tj>Sod1i* testis. The depletion
245 of Sod1 in CySC resulted in elevated expression of Hh receptor, Patched (Ptc) (Fig.
246 4I, S4V) which extended to regions farther from the hub, overlapping with expanded
247 Tj^+ cells (Fig. 4G and H). Since, Ptc itself is a transcriptional Hh target, its expression
248 in CySCs suggests active Hh signalling[45], further supported by higher levels and a
249 similar pattern of Hh transcriptional effector, Cubitus interruptus (Ci), in *Sod1i* testis
250 (Fig. 4M'', N'', J and S4W). Since, Ptc, Ci, and a GPCR-like signal transducer
251 Smoothened (Smo) are all transcriptionally driven by Hh, and Hh itself is regulated by
252 higher levels of Ci[46,47], we expectedly found higher levels of transcripts for these
253 pathway genes (Fig. S4C-F). The overt proliferation of CySCs under high ROS
254 conditions was suppressed by reducing hh mRNA levels in hub cells and CySCs using
255 *Hh-RNAi* (Fig. 4L and Fig. S4G-I), which also rescued the GSC population (Fig. 4K
256 and S4J-L). The levels of Sod1 transcripts under depletion of Sod1 alone and Sod1,
257 hh double knock-down were almost similar (Fig. S4M). To determine whether the
258 changes observed in the germ cell population were a sole consequence of *Sod1*
259 knockdown in CySC, we manipulated CySC numbers using *UAS-Ci* and assessed
260 their impact on neighbouring GSCs. Ci overexpression driven by *Tj-Gal4* led to a
261 higher number of Tj^+ cells (Fig. S4N, R'' and S-U) and a complete loss of $Vasa^+$ GSCs
262 (Fig. S4O, and R'''). However, the effect on CySC and GSC population was less
263 severe when driven by *C-587 Gal4* (Fig.S4N, O, Q''and Q''').

264

265 **Elevating CySC antioxidant defence promotes GSC self-renewal**

266 To further substantiate the role of ROS in coordinating the stem cell populations, we
267 strengthened the cellular defences against oxidants by overexpressing Sod1 in
268 CySCs. We checked the overall ROS level using DHE (Fig. S5I) and monitored the
269 relative GSC/CySC populations. Together with reduction in superoxide levels, we
270 observed an increase in the number of $Vasa^+$ cells (Fig. 5A and S5A''-B''), and a slight
271 reduction in Tj^+ cells (Fig. 5B and S5E''-F''). Any morphological anomalies associated
272 with cell-cell adhesion or abnormal cellular dispersion, was not observed (Fig. S5A-B
273 and E-F). Enhancing the levels of Sod1 in GSCs promoted the growth of GSC-like
274 cells (Fig. S5C'', D'' and J) but did not have any prominent effect on CySCs (Fig. S5G'',

275 H'' and K). The increment in Vasa$^+$ GSCs under CySC-induced low redox conditions
276 was also represented by a parallel increase in spectrosome number (Fig. 5C-E). The
277 uptick in GSC number due to scavenging of ROS in CySC, might be a result of delayed
278 differentiation, as indicated by displacement of Bam$^+$ zone away from hub; thus,
279 confirming non-cell-autonomous role of CySC ROS in maintaining GSC fate (Fig. 5F-
280 H). The data suggest that reducing redox profile of CySCs differentially affected their
281 own self-renewing propensities along with GSC maintenance and optimum redox state
282 of both the stem-cell populations is controlled by CySCs.

283

284 **Discussion:**

285 ROS is a crucial mediator of stem cell maintenance where these species act as second
286 messengers to induce different post-translational protein modifications thereby,
287 affecting cell fate[48,49]. The effect of ROS is mainly considered to be autocrine in nature,
288 where generation of these oxidative species is usually restricted to specific cellular
289 compartments, ensuring they act close to their targets. Recent studies have reported
290 non-autonomous generation of ROS by NOX enzymes or upon stimulation by growth
291 factors, to play a critical role in regenerative growth[50-52]. However, in either case, the
292 target cell serves as both the source and the site of response. Among ROS, hydrogen
293 peroxide (H_2O_2) stands out due to its stability and membrane permeability[53], allowing
294 it to diffuse from its source[54]. Non-myocytic pericardial cells (PCs) in *Drosophila* exhibit
295 elevated ROS that act in a paracrine manner to influence adjacent cardiomyocytes
296 (CMs) not by direct diffusion but through activation of the D-p38 MAPK cascade within
297 PCs[55]. In cardiomyocyte monolayers, wounding induces H_2O_2 and superoxide
298 accumulation that propagate via gap junctions, creating a cell-to-cell ROS wave where
299 even distant cells show increased cytosolic H_2O_2 and altered proteomes[56]. Together,
300 these findings suggest that ROS can spread between cells either by direct
301 diffusion/gap-junctional transfer or indirectly by modulating signaling cascades and
302 secreted factors. Our findings indicate that CySCs due to their high baseline ROS
303 levels, affect the redox state of their neighbourhood including GSCs. ROS imbalance
304 in CySCs enhance the oxidative levels of their surrounding that is, GSC that cause
305 them to differentiate. High ROS mediated differentiation of GSCs has already been
306 reported earlier[17] and depletion of superoxide dismutases in GSCs did result in

307 reduction of their number. However, perturbation of ROS in GSCs did not have
308 significant effect on CySC population. This shows that cell non-autonomous effect of
309 ROS is observed only when it originates from CySCs.

310 Our observations in *Drosophila* testicular stem cell niche suggested a previously
311 unaccounted role of superoxide dismutases in maintaining niche homoeostasis. The
312 redox perturbations affected cyst stem cell dynamics which indirectly influenced the
313 germline. The higher ROS threshold of CySCs maintained the physiological redox
314 state of GSCs. Reduced ROS in GSC was accompanied with its proliferation[57],
315 phenocopied when Sod1 was overexpressed in its neighbours (Fig. 5). However, we
316 feel that net alterations in GSC state were the combinatorial effect of oxidative stress
317 and niche alterations brought about by CySC deregulation.

318 GSCs are anchored to the hub cells via adherens junctions, allowing them to receive
319 crucial maintenance signals[28]. These include Bone Morphogenetic Proteins (BMPs)
320 such as Decapentaplegic (Dpp) and Glass bottom boat (Gbb), which activate the BMP
321 pathway[31] required for GSC self-renewal, and Unpaired (Upd), which triggers the JAK-
322 STAT pathway to promote GSC adhesion to the hub[58]. The suppression of these
323 pathways activates Bam, acting as a switch from transit-amplifying cells to
324 spermatocyte differentiation[59,60]. Elevated ROS in CySC possibly affected STAT
325 phosphorylation through S-glutathionylation[61,62], reducing the levels of STAT-
326 dependent transcripts such as Socs36E[63], Ptp61F and E-cadherin. This depletion
327 compromises GSC adhesion, resulting in detachment from neighboring cells, similar
328 to E-cadherin loss conditions [58,64-66]. This resulted in compromised GSC-CySC
329 paracrine receptions such as EGFR which play a crucial role in the maintenance of
330 cell-polarity that segregates self-renewing CySC populations from the ones receiving
331 differentiation cues [44,67,68], leading to the accumulation of cells co-expressing both
332 stemness and differentiation markers. In contrast to GSCs, ROS imbalance in CySCs
333 induced accelerated proliferation as well as differentiation due to deregulation of
334 EGFR and Hedgehog pathways. Although, redox modulation of EGFR pathway
335 components has been previously demonstrated[69], in this study we found Hedgehog to
336 be probably susceptible to redox regulation. The redox dependent induction of
337 Hedgehog probably, contributed to enhancement in CySC numbers which partly
338 contributed to depletion of GSCs.

However, we do not rule out the possibility of hub cells playing an equivalent role in GSC maintenance, given their parallel effect in suppressing GSC differentiation[30]. Tj majorly expresses in CySCs but also shows modest expression in hub. Therefore, the possible depletion of Sod1 in both hub and CySCs by *Tj-Gal4* together with, demonstration of a stronger phenotype in *Tj-Sod1RNAi* testis compared to CySC specific *C587-Sod1RNAi*, indicated potential hub contributions in CySC self-renewal. While ROS accumulation typically enhances EGFR signaling promoting premature GSC differentiation[70], the loss of EGFR in somatic cells increases the number of GSCs[67] and is associated with fewer somatic cells [71]. However, we observed that Sod1 depletion caused parallel reduction of both pErk levels and GSC number. It is quite possible that the response of germline to Erk modulation is more context-dependent which is influenced by other receptor tyrosin kinases beyond EGFR. To test this hypothesis, we had tried an EGFR gain-of-function rescue of CySC depletion but the driven progenies were lethal in the absence of Sod1. We also avoided usage of Gal80 dependent clonal populations to maintain a homogenous genetic background and prevent false readouts due to diffusion of ROS signals in unaltered neighbourhood.

The proposed concept of intercellular ROS communication can be of importance in deciphering the biochemical adaptability and plasticity of different niches influencing stem cell fate, ensuring niche size and architecture to prevent stem cell loss and aging. This has been observed in neural stem cells where inflammation-induced quiescence recovers the regenerating capacity of aging brain[72]. In addition to metabolic variations, dependence of the germline on somatic neighbours for its redox state might be one the reasons behind its presumed immortal nature and resistance to aging[73]. The same can also be applied to cancer stem cells, which maintain niche occupancy and resist oxidative stress-induced apoptosis, probably by receiving redox cues from the environment. However, further work is required to elucidate the myriads of driver mechanisms intersecting in the realm of redox regulation that extend beyond the present system into broader translational areas.

370 **Materials and Methods**

371 **Fly strains**

372 Fly stocks were maintained and crosses were set at 25°C on normal corn meal and
373 yeast medium unless otherwise indicated. All fly stocks (BL-24493) *UAS SOD1 RNAi*,
374 (BL-32909) *UAS SOD1 RNAi*, (BL-29389) *UAS SOD1 RNAi*, (BL-32983) *UAS SOD2*
375 *RNAi*, (BL-24754) *UAS SOD1*, (BL- 32489) *UAS hhRNAi*, (BL- 25751) *UAS Dcr-nos*
376 *Gal4*, (BL-55122) *UAS-FUCCI*, were obtained from Bloomington Drosophila Stock
377 Centre. *Nos-Gal4*, *Tj-Gal4*, *Tj-Gal4-BamGFP*, *gstD1-GFP*, *TFAM-GFP, UAS-Ci* were
378 kind gift from U. Nongthomba, P. Majumder, K. Ray, B. C. Mandal, Hong Xu, LS
379 Shahidhara labs respectively. Parents were maintained at 25°C, and crosses were set
380 at the same temperature. To ensure optimal Gal4 activity, progenies were shifted to
381 29°C until eclosion, with aging also conducted at 29°C. Males aged 3–5 days were
382 used for all experiments. The control lines for all experiments are the corresponding
383 Gal4-line crossed with wild type *OregonR*$^{+}$.

384

385 **Dissection and immunostaining**

386 Anesthetized flies were dissected in 1X Phosphate Buffer Saline (PBS). All incubations
387 were carried out at room temperature (25°C) unless otherwise mentioned. Testes were
388 fixed in 4% paraformaldehyde for 30 minutes, followed by three washes with 0.3%
389 PBTX (PBS + TritonX 100). Post-blocking in 0.5% Bovine Serum Albumin, testis was
390 incubated overnight at 4°C for primary antisera, followed by washing in 0.3% PBTX 3
391 times 15 minutes each before incubating with secondary antibody. The tissues were
392 counterstained with DAPI (4,6-diamidino-2-phenylindole) for 20 minutes, followed by
393 three washes in 0.3% PBTX for 15 minutes each. For Patched antibody staining, a
394 modified protocol utilizing PIPES-EGTA buffer was used as described[74]. For Eya
395 staining, the tissues were incubated in primary antibody for 2 days. The dpErk was
396 labelled by dissecting fly testes in Schneider's media, followed by fixation in 4% PFA
397 for 30 min, 3x wash in 0.1% PBTX, blocked and incubated in primary antibody
398 overnight; each step supplemented with phosphatase inhibitor cocktail 2 (1:100,
399 Sigma, cat#P5726). Samples were mounted in DABCO anti-fade medium prior
400 imaging.

401 The following primary antibodies were used in the experiments - anti-FasIII (7G10)
402 (1:120, DSHB (Developmental Studies Hybridoma Bank)), anti-Eya (1:50, DSHB),
403 anti-DEcad (DCAD2) (1:50, DSHB), anti-α-Spectrin (3A9) (1:20, DSHB), anti-Ptc
404 (1:50,DSHB) , anti-Ci (1:50, DSHB), anti -Dlg (1:50), anti-βtubulin (1:300, DSHB), anti-
405 pERK (1:100, Cell Signaling (4370)), ATP5A (1:700, Abcam (ab14748)), anti-Tj
406 (1:5000), anti-Vasa (1:4000), anti-Zfh1(1:2000). The primary labelling was detected
407 using appropriate Alexa-Flour tagged secondary antibody (ThermoFisher Scientific).

408 To assess superoxide levels, testes were dissected in Schneider's medium (SM) and
409 immediately incubated in 30 µM Dihydroxyethidium (DHE) at 25 °C in the dark. Testes
410 were washed thrice with SM for 7 minutes each before quantifying the emitted
411 fluorescence using SpectraMax iD5 (Molecular Devices).

412

413 **Quantitative Reverse transcription–PCR**

414 For semi-quantitative RT-PCR and qRT-PCR analyses, total RNA was isolated from
415 testes of 3-5 days old male flies using Qiagen RNA extraction kit. RNA pellets were
416 resuspended in nuclease-free water and quantity of RNA was spectrophotometrically
417 estimated. First-strand cDNA was synthesized from 1-2 µg of total RNA as described
418 earlier. The prepared cDNAs were subjected to real time PCR using forward and
419 reverse primer pairs as listed below, using 5 µl qPCR Master Mix (SYBR Green,
420 ThermoFisher Scientific), 2 pmol/µl of each primer per reaction for 10 µl final volume
421 in ABI 7500 Real time PCR machine. The fold change in expression was calculated
422 through $2^{-\Delta\Delta Ct}$ method. The primers used are listed in Supplementary Table S1.

423

424 **Imaging and image analysis**

425 Confocal imaging was carried out using Zeiss LSM 900 confocal microscope, using
426 appropriate dichroics and filters. Images were further analyzed and processed for
427 brightness and contrast adjustments using ImageJ (Fiji). Mean intensity
428 measurements were carried out using standard Fiji plug-ins,The relative distance from
429 the two reference points in the images was estimated through Inter-edge Distance
430 ImageJ Macro v2.0 from Github. All images were assembled using Adobe Photoshop
431 version 21.2.1.

432

433 **Quantification of GSCs, CySCs and CCs**

434 For GSC quantification, only cells in direct contact with the hub were considered. While
435 single slices are shown for representation, counting was performed on individual slices
436 of z-stacks using the semi-automated Cell Counter plugin in Fiji for all specified
437 genotypes.

438 For CySC quantification, all Tj-positive and Zfh1-positive cells present in each testis
439 were counted and represented. For cyst cells quantification, only those near the hub
440 were considered, which does not reflect the total number of Eya-positive cells. All
441 quantifications were performed using the Cell Counter plugin in Fiji.

442

443 **Mitochondrial and *gstD1*-GFP quantification:** The mitochondrial analyzer first
444 generates 2D mitochondrial regions of interest (ROIs), followed by the measurement
445 of their total area and circularity. Initially, this is done using a thresholded image of a
446 single slice. For *gstD1*-GFP quantification**,** we have quantified the region of *gstD1*-
447 GFP that overlapped with Vasa-positive germ cells which are in direct contact with hub
448 to assess the presence of ROS reporter signal within the germline compartment. To
449 ensure accurate cell boundary demarcation, we used Dlg staining as an additional
450 parameter.

451

452 **Immunoblot Analysis**

453 Protein was extracted from the dissected testes using RIPA buffer as described
454 previously and quantified using Bradford reagent (Biorad). Equivalent concentration of
455 lysate was denatured using 1X Laemelli Buffer with 1 M DTT at 95°C, separated in
456 10% SDS-PAGE and transferred onto PVDF membranes. Membranes were blocked
457 with commercial blocking solution in TBST base before sequential primary antibody
458 incubation with anti-Vasa and anti-β-Tubulin (DSHB, E7). Secondary detection was
459 performed using HRP-tag anti-mouse antibody (GE Amersham).

460

461 **Statistical analyses**

462 The sample sizes carrying adequate statistical power are mentioned in the figure
463 legends. Statistical significance for each experiment was calculated using two-tailed
464 Student's t-test, unless otherwise mentioned, using GraphPad Prism 8 software. The
465 *P* values were calculated through pairwise comparison of the data with wild type or
466 driver alone and driven RNAi lines. Significance values for sample sizes mentioned in
467 figure legends were represented as $*P < 0.01$, $**P < 0.001$, or $***P < 0.0001$.
468
469
470 **Author contribution**
471 D.S. and O.M conceived the study and designed the experiments. O.M, A.C and T.C
472 performed the experiments. D.S and O.M analyzed the data. D.S, O.M. and A.C. wrote
473 the manuscript.
474
475 **Acknowledgements**
476 We thank P. Majumder, U. Nongthomba, K. Ray, G. Ratnaparkhi, B. C. Mandal, Hong
477 Xu lab and S. C. Lakhotia for kindly sharing some of the transgenic fly lines. Christian
478 Bökel for sharing experimental protocols. Anti-Tj antibody was a generous gift from
479 Prof. D. Godt, University of Toronto. Anti-Vasa and Anti-Zfh1 were kindly gifted by
480 Prof. R. Lehmann, New York University. We also thank Dr. Bama Charan Mandal for
481 generously sharing his Confocal microscope imaging system and Sudeshna
482 Majumder for preliminary data. We acknowledge BDSC for fly stocks and DSHB for
483 antibodies. This work is supported by Innovative Young Biotechnologist Award by
484 Department of Biotechnology (BT/12/IYBA/2019/01), Early Career Research Award
485 by Science and Engineering Research Board (ECR/2018/000009), BHU-Institute of
486 Eminence grant (R/Dev/IoE/Incentive/2021-22/32452). The authors also acknowledge
487 financial support from DST-INSPIRE fellowship (to O.M.) and UGC-CAS doctoral
488 fellowship (to T.C.).
489
490 **Declaration of interest**
491 The authors declare no competing interests.
492
493
494 **Data availability**

The data that support the findings of this study are available within the main text and its Supplementary Information file. The lead contact will share all raw data associated with this paper upon request. This study did not utilize or generate any unique datasets or codes.

References

1 Schieber, M. & Chandel, N. S. ROS function in redox signaling and oxidative stress. *Curr Biol* **24**, R453-462, doi:10.1016/j.cub.2014.03.034 (2014).

2 Holmstrom, K. M. & Finkel, T. Cellular mechanisms and physiological consequences of redox-dependent signalling. *Nat Rev Mol Cell Biol* **15**, 411-421, doi:10.1038/nrm3801 (2014).

3 D'Autreaux, B. & Toledano, M. B. ROS as signalling molecules: mechanisms that generate specificity in ROS homeostasis. *Nat Rev Mol Cell Biol* **8**, 813-824, doi:10.1038/nrm2256 (2007).

4 Maryanovich, M. & Gross, A. A ROS rheostat for cell fate regulation. *Trends Cell Biol* **23**, 129-134, doi:10.1016/j.tcb.2012.09.007 (2013).

5 Murphy, M. P. How mitochondria produce reactive oxygen species. *Biochem J* **417**, 1-13, doi:10.1042/BJ20081386 (2009).

6 Hamanaka, R. B. & Chandel, N. S. Mitochondrial reactive oxygen species regulate cellular signaling and dictate biological outcomes. *Trends Biochem Sci* **35**, 505-513, doi:10.1016/j.tibs.2010.04.002 (2010).

7 Al-Mehdi, A. B. *et al.* Perinuclear mitochondrial clustering creates an oxidant-rich nuclear domain required for hypoxia-induced transcription. *Sci Signal* **5**, ra47, doi:10.1126/scisignal.2002712 (2012).

8 Bedard, K. & Krause, K. H. The NOX family of ROS-generating NADPH oxidases: physiology and pathophysiology. *Physiol Rev* **87**, 245-313, doi:10.1152/physrev.00044.2005 (2007).

9 Appenzeller-Herzog, C. *et al.* Transit of H2O2 across the endoplasmic reticulum membrane is not sluggish. *Free Radic Biol Med* **94**, 157-160, doi:10.1016/j.freeradbiomed.2016.02.030 (2016).

10 Mishina, N. M. *et al.* Which Antioxidant System Shapes Intracellular H(2)O(2) Gradients? *Antioxid Redox Signal* **31**, 664-670, doi:10.1089/ars.2018.7697 (2019).

11 Yoboue, E. D., Sitia, R. & Simmen, T. Redox crosstalk at endoplasmic reticulum (ER) membrane contact sites (MCS) uses toxic waste to deliver messages. *Cell Death Dis* **9**, 331, doi:10.1038/s41419-017-0033-4 (2018).

12 Rehman, J. Empowering self-renewal and differentiation: the role of mitochondria in stem cells. *J Mol Med (Berl)* **88**, 981-986, doi:10.1007/s00109-010-0678-2 (2010).

13 Li, T. S. & Marban, E. Physiological levels of reactive oxygen species are required to maintain genomic stability in stem cells. *Stem Cells* **28**, 1178-1185, doi:10.1002/stem.438 (2010).

14 Le Belle, J. E. *et al.* Proliferative neural stem cells have high endogenous ROS levels that regulate self-renewal and neurogenesis in a PI3K/Akt-dependant manner. *Cell Stem Cell* **8**, 59-71, doi:10.1016/j.stem.2010.11.028 (2011).

15 Chuikov, S., Levi, B. P., Smith, M. L. & Morrison, S. J. Prdm16 promotes stem cell maintenance in multiple tissues, partly by regulating oxidative stress. *Nat Cell Biol* **12**, 999-1006, doi:10.1038/ncb2101 (2010).

16 Owusu-Ansah, E. & Banerjee, U. Reactive oxygen species prime Drosophila haematopoietic progenitors for differentiation. *Nature* **461**, 537-541, doi:10.1038/nature08313 (2009).

17 Tan, S. W. S., Lee, Q. Y., Wong, B. S. E., Cai, Y. & Baeg, G. H. Redox Homeostasis Plays Important Roles in the Maintenance of the Drosophila Testis Germline Stem Cells. *Stem Cell Reports* **9**, 342-354, doi:10.1016/j.stemcr.2017.05.034 (2017).

18 Zhou, G., Meng, S., Li, Y., Ghebre, Y. T. & Cooke, J. P. Optimal ROS Signaling Is Critical for Nuclear Reprogramming. *Cell Rep* **15**, 919-925, doi:10.1016/j.celrep.2016.03.084 (2016).

19 Morris, O. & Jasper, H. Reactive Oxygen Species in intestinal stem cell metabolism, fate and function. *Free Radic Biol Med* **166**, 140-146, doi:10.1016/j.freeradbiomed.2021.02.015 (2021).

20 Sinenko, S. A., Shim, J. & Banerjee, U. Oxidative stress in the haematopoietic niche regulates the cellular immune response in Drosophila. *EMBO Rep* **13**, 83-89, doi:10.1038/embor.2011.223 (2011).

21 Davies, E. L. & Fuller, M. T. Regulation of self-renewal and differentiation in adult stem cell lineages: lessons from the Drosophila male germ line. *Cold Spring Harb Symp Quant Biol* **73**, 137-145, doi:10.1101/sqb.2008.73.063 (2008).

22 Hime, G. R., Brill, J. A. & Fuller, M. T. Assembly of ring canals in the male germ line from structural components of the contractile ring. *J Cell Sci* **109 (Pt 12)**, 2779-2788, doi:10.1242/jcs.109.12.2779 (1996).

23 Gonczy, P. & DiNardo, S. The germ line regulates somatic cyst cell proliferation and fate during Drosophila spermatogenesis. *Development* **122**, 2437-2447, doi:10.1242/dev.122.8.2437 (1996).

24 Fabrizio, J. J., Boyle, M. & DiNardo, S. A somatic role for eyes absent (eya) and sine oculis (so) in Drosophila spermatocyte development. *Dev Biol* **258**, 117-128, doi:10.1016/s0012-1606(03)00127-1 (2003).

25 Hardy, R. W., Tokuyasu, K. T., Lindsley, D. L. & Garavito, M. The germinal proliferation center in the testis of Drosophila melanogaster. *J Ultrastruct Res* **69**, 180-190, doi:10.1016/s0022-5320(79)90108-4 (1979).

26 Chen, S., Lewallen, M. & Xie, T. Adhesion in the stem cell niche: biological roles and regulation. *Development* **140**, 255-265, doi:10.1242/dev.083139 (2013).

27 Inaba, M., Yuan, H., Salzmann, V., Fuller, M. T. & Yamashita, Y. M. E-cadherin is required for centrosome and spindle orientation in Drosophila male germline stem cells. *PLoS One* **5**, e12473, doi:10.1371/journal.pone.0012473 (2010).

28 Greenspan, L. J., de Cuevas, M. & Matunis, E. Genetics of gonadal stem cell renewal. *Annu Rev Cell Dev Biol* **31**, 291-315, doi:10.1146/annurev-cellbio-100913-013344 (2015).

29 Kiger, A. A., Jones, D. L., Schulz, C., Rogers, M. B. & Fuller, M. T. Stem cell self-renewal specified by JAK-STAT activation in response to a support cell cue. *Science* **294**, 2542-2545, doi:10.1126/science.1066707 (2001).

30 Tulina, N. & Matunis, E. Control of stem cell self-renewal in Drosophila spermatogenesis by JAK-STAT signaling. *Science* **294**, 2546-2549, doi:10.1126/science.1066700 (2001).

31 Kawase, E., Wong, M. D., Ding, B. C. & Xie, T. Gbb/Bmp signaling is essential for maintaining germline stem cells and for repressing bam transcription in the Drosophila testis. *Development* **131**, 1365-1375, doi:10.1242/dev.01025 (2004).

32 Michel, M., Kupinski, A. P., Raabe, I. & Bokel, C. Hh signalling is essential for somatic stem cell maintenance in the Drosophila testis niche. *Development* **139**, 2663-2669, doi:10.1242/dev.075242 (2012).

33 Song, X. *et al.* Bmp signals from niche cells directly repress transcription of a differentiation-promoting gene, bag of marbles, in germline stem cells in the Drosophila ovary. *Development* **131**, 1353-1364, doi:10.1242/dev.01026 (2004).

34 Losick, V. P., Morris, L. X., Fox, D. T. & Spradling, A. Drosophila stem cell niches: a decade of discovery suggests a unified view of stem cell regulation. *Dev Cell* **21**, 159-171, doi:10.1016/j.devcel.2011.06.018 (2011).

589 35 Lenhart, K. F. & DiNardo, S. Somatic cell encystment promotes abscission in germline stem cells
590 following a regulated block in cytokinesis. *Dev Cell* **34**, 192-205,
591 doi:10.1016/j.devcel.2015.05.003 (2015).
592 36 Jemc, J. C. Somatic gonadal cells: the supporting cast for the germline. *Genesis* **49**, 753-775,
593 doi:10.1002/dvg.20784 (2011).
594 37 Zoller, R. & Schulz, C. The Drosophila cyst stem cell lineage: Partners behind the scenes?
595 *Spermatogenesis* **2**, 145-157, doi:10.4161/spmg.21380 (2012).
596 38 Larsson, N. G. *et al.* Mitochondrial transcription factor A is necessary for mtDNA maintenance
597 and embryogenesis in mice. *Nat Genet* **18**, 231-236, doi:10.1038/ng0398-231 (1998).
598 39 Sykiotis, G. P. & Bohmann, D. Keap1/Nrf2 signaling regulates oxidative stress tolerance and
599 lifespan in Drosophila. *Dev Cell* **14**, 76-85, doi:10.1016/j.devcel.2007.12.002 (2008).
600 40 Fairchild, M. J., Yang, L., Goodwin, K. & Tanentzapf, G. Occluding Junctions Maintain Stem Cell
601 Niche Homeostasis in the Fly Testes. *Curr Biol* **26**, 2492-2499, doi:10.1016/j.cub.2016.07.012
602 (2016).
603 41 Zielke, N. *et al.* Fly-FUCCI: A versatile tool for studying cell proliferation in complex tissues. *Cell*
604 *Rep* **7**, 588-598, doi:10.1016/j.celrep.2014.03.020 (2014).
605 42 Ng, C. L., Qian, Y. & Schulz, C. Notch and Delta are required for survival of the germline stem
606 cell lineage in testes of Drosophila melanogaster. *PLoS One* **14**, e0222471,
607 doi:10.1371/journal.pone.0222471 (2019).
608 43 Amoyel, M., Hillion, K. H., Margolis, S. R. & Bach, E. A. Somatic stem cell differentiation is
609 regulated by PI3K/Tor signaling in response to local cues. *Development* **143**, 3914-3925,
610 doi:10.1242/dev.139782 (2016).
611 44 Castanieto, A., Johnston, M. J. & Nystul, T. G. EGFR signaling promotes self-renewal through
612 the establishment of cell polarity in Drosophila follicle stem cells. *Elife* **3**,
613 doi:10.7554/eLife.04437 (2014).
614 45 Chen, Y. & Struhl, G. Dual roles for patched in sequestering and transducing Hedgehog. *Cell* **87**,
615 553-563, doi:10.1016/s0092-8674(00)81374-4 (1996).
616 46 Chen, Y. & Struhl, G. In vivo evidence that Patched and Smoothened constitute distinct binding
617 and transducing components of a Hedgehog receptor complex. *Development* **125**, 4943-4948,
618 doi:10.1242/dev.125.24.4943 (1998).
619 47 Jiang, J. & Hui, C. C. Hedgehog signaling in development and cancer. *Dev Cell* **15**, 801-812,
620 doi:10.1016/j.devcel.2008.11.010 (2008).
621 48 Sinenko, S. A., Starkova, T. Y., Kuzmin, A. A. & Tomilin, A. N. Physiological Signaling Functions
622 of Reactive Oxygen Species in Stem Cells: From Flies to Man. *Front Cell Dev Biol* **9**, 714370,
623 doi:10.3389/fcell.2021.714370 (2021).
624 49 Liang, R. & Ghaffari, S. Stem cells, redox signaling, and stem cell aging. *Antioxid Redox Signal*
625 **20**, 1902-1916, doi:10.1089/ars.2013.5300 (2014).
626 50 Fu, X. J. *et al.* NADPH oxidase 1 and its derived reactive oxygen species mediated tissue injury
627 and repair. *Oxid Med Cell Longev* **2014**, 282854, doi:10.1155/2014/282854 (2014).
628 51 Taylor-Fishwick, D. A. NOX, NOX Who is There? The Contribution of NADPH Oxidase One to
629 Beta Cell Dysfunction. *Front Endocrinol (Lausanne)* **4**, 40, doi:10.3389/fendo.2013.00040
630 (2013).
631 52 Santabarbara-Ruiz, P. *et al.* Ask1 and Akt act synergistically to promote ROS-dependent
632 regeneration in Drosophila. *PLoS Genet* **15**, e1007926, doi:10.1371/journal.pgen.1007926
633 (2019).
634 53 Bienert, G. P. *et al.* Specific aquaporins facilitate the diffusion of hydrogen peroxide across
635 membranes. *J Biol Chem* **282**, 1183-1192, doi:10.1074/jbc.M603761200 (2007).
636 54 Milkovic, L., Cipak Gasparovic, A., Cindric, M., Mouthuy, P. A. & Zarkovic, N. Short Overview of
637 ROS as Cell Function Regulators and Their Implications in Therapy Concepts. *Cells* **8**,
638 doi:10.3390/cells8080793 (2019).

55 Lim, H. Y., Wang, W., Chen, J., Ocorr, K. & Bodmer, R. ROS regulate cardiac function via a distinct paracrine mechanism. *Cell Rep* **7**, 35-44, doi:10.1016/j.celrep.2014.02.029 (2014).
56 Fichman, Y., Rowland, L., Nguyen, T. T., Chen, S. J. & Mittler, R. Propagation of a rapid cell-to-cell H(2)O(2) signal over long distances in a monolayer of cardiomyocyte cells. *Redox Biol* **70**, 103069, doi:10.1016/j.redox.2024.103069 (2024).
57 Pan, L. *et al.* Stem cell aging is controlled both intrinsically and extrinsically in the Drosophila ovary. *Cell Stem Cell* **1**, 458-469, doi:10.1016/j.stem.2007.09.010 (2007).
58 Leatherman, J. L. & Dinardo, S. Germline self-renewal requires cyst stem cells and stat regulates niche adhesion in Drosophila testes. *Nat Cell Biol* **12**, 806-811, doi:10.1038/ncb2086 (2010).
59 Bausek, N. JAK-STAT signaling in stem cells and their niches in Drosophila. *JAKSTAT* **2**, e25686, doi:10.4161/jkst.25686 (2013).
60 Gonczy, P., Matunis, E. & DiNardo, S. bag-of-marbles and benign gonial cell neoplasm act in the germline to restrict proliferation during Drosophila spermatogenesis. *Development* **124**, 4361-4371, doi:10.1242/dev.124.21.4361 (1997).
61 Butturini, E. *et al.* S-Glutathionylation at Cys328 and Cys542 impairs STAT3 phosphorylation. *ACS Chem Biol* **9**, 1885-1893, doi:10.1021/cb500407d (2014).
62 Xiong, Y., Uys, J. D., Tew, K. D. & Townsend, D. M. S-glutathionylation: from molecular mechanisms to health outcomes. *Antioxid Redox Signal* **15**, 233-270, doi:10.1089/ars.2010.3540 (2011).
63 Issigonis, M. *et al.* JAK-STAT signal inhibition regulates competition in the Drosophila testis stem cell niche. *Science* **326**, 153-156, doi:10.1126/science.1176817 (2009).
64 DeGennaro, M. *et al.* Peroxiredoxin stabilization of DE-cadherin promotes primordial germ cell adhesion. *Dev Cell* **20**, 233-243, doi:10.1016/j.devcel.2010.12.007 (2011).
65 Karsten, P., Hader, S. & Zeidler, M. P. Cloning and expression of Drosophila SOCS36E and its potential regulation by the JAK/STAT pathway. *Mech Dev* **117**, 343-346, doi:10.1016/s0925-4773(02)00216-2 (2002).
66 Richmond, C. A. *et al.* JAK/STAT-1 Signaling Is Required for Reserve Intestinal Stem Cell Activation during Intestinal Regeneration Following Acute Inflammation. *Stem Cell Reports* **10**, 17-26, doi:10.1016/j.stemcr.2017.11.015 (2018).
67 Kiger, A. A., White-Cooper, H. & Fuller, M. T. Somatic support cells restrict germline stem cell self-renewal and promote differentiation. *Nature* **407**, 750-754, doi:10.1038/35037606 (2000).
68 Schulz, C., Wood, C. G., Jones, D. L., Tazuke, S. I. & Fuller, M. T. Signaling from germ cells mediated by the rhomboid homolog stet organizes encapsulation by somatic support cells. *Development* **129**, 4523-4534, doi:10.1242/dev.129.19.4523 (2002).
69 Koundouros, N. & Poulogiannis, G. Phosphoinositide 3-Kinase/Akt Signaling and Redox Metabolism in Cancer. *Front Oncol* **8**, 160, doi:10.3389/fonc.2018.00160 (2018).
70 Senos Demarco, R. & Jones, D. L. Mitochondrial fission regulates germ cell differentiation by suppressing ROS-mediated activation of Epidermal Growth Factor Signaling in the Drosophila larval testis. *Sci Rep* **9**, 19695, doi:10.1038/s41598-019-55728-0 (2019).
71 Amoyel, M., Anderson, J., Suisse, A., Glasner, J. & Bach, E. A. Socs36E Controls Niche Competition by Repressing MAPK Signaling in the Drosophila Testis. *PLoS Genet* **12**, e1005815, doi:10.1371/journal.pgen.1005815 (2016).
72 Kalamakis, G. *et al.* Quiescence Modulates Stem Cell Maintenance and Regenerative Capacity in the Aging Brain. *Cell* **176**, 1407-1419 e1414, doi:10.1016/j.cell.2019.01.040 (2019).
73 Snoeck, H. W. Can Metabolic Mechanisms of Stem Cell Maintenance Explain Aging and the Immortal Germline? *Cell Stem Cell* **16**, 582-584, doi:10.1016/j.stem.2015.04.021 (2015).
74 Michel, M., Raabe, I., Kupinski, A. P., Perez-Palencia, R. & Bokel, C. Local BMP receptor activation at adherens junctions in the Drosophila germline stem cell niche. *Nat Commun* **2**, 415, doi:10.1038/ncomms1426 (2011).

690

691

692 **Figure Legends**

693 **Figure 1. Mitochondrial Distribution and Redox Profile of GSCs and CySCs in**
694 **Adult *Drosophila* Testes**

695 (A) Schematic representation of adult *Drosophila* testicular niche showing
696 arrangement of different stem cell populations (GSC – Germinal Stem Cell, CySC –
697 Cyst Stem Cell). (B-E) Differential distribution of mitochondria labelled with ATP5A
698 (monochrome/green) in Vasa^{+} GSCs of wild-type fly testis with cellular boundaries
699 marked by Dlg; B# shows digitally zoomed image of the dotted area of B. (F)
700 Quantification of mitochondrial area per cell. Bars represent mean ± s.e.m., n = 10
701 fields of view; ****P (unpaired t-test)<0.0001.* (G-P) Redox profiling of testicular stem
702 cell niche using *gstD1*-GFP as intrinsic ROS reporter in control (G-K) and *Tj-Gal4*
703 driven *Sod1RNAi (Sod1i)* testis (L-P). Dotted area denotes the region of CySC
704 occupancy and asterisk denotes the hub. (Q) Quantification of *gstD1*-GFP mean
705 fluorescence intensity (MFI) represented as fold change between GSCs and CySCs
706 in controls. Data denotes mean ± s.e.m,, n = 25, ****P(unpaired t-test)<0.0001.* (R)
707 Quantification of cell-specific ROS content upon *Sod1RNAi*. Data denotes mean ±
708 s.e.m, n = 25, ****P(unpaired t-test)<0.0001.* Controls are the indicated driver line
709 crossed with *Oregon R*$^{+}$. Scale bar - 10 µm. See also Figure S1.

710

711 **Figure 2. Redox disequilibrium in Cyst stem cell lineage deregulates early**
712 **CySCs and decreases the GSC number**

713 (A-B) Distribution of Tj^{+} CySC/early cyst cell around the hub (FasIII) in control and Tj
714 driven *Sod1RNAi* testis. (C-D) Represents the rosette arrangement of Vasa^{+} GSCs
715 flanking the hub (dotted area). (E-G) Mean number of Tj^{+} cells, Zfh1^{+} early CySCs and
716 GSCs in control and *Sod1RNAi* lines shown as mean ± s.e.m, n = 10, ****P(unpaired*
717 *t-test)<0.0001, **P(unpaired t-test)<0.0001.* (H) Construct design of the FUCCI
718 reporter line for tracking the cell cycle stages in *Drosophila* tissues, containing degrons
719 of Cyclin B and E2F1 proteins fused with RFP or GFP. G1, S and G2/M is represented
720 by GFP^{+}, RFP^{+} and dual labelled cells respectively. (I-J) Comparative changes in the

721 cell cycle phases (I) or Zfh1^{+} cells (J) present in G1, S and G2/M phase at the niche
722 zone between control and *Tj>Sod1i*. Data denote mean ± s.e.m, n = 10, ****P(unpaired*
723 *t-test)<0.0001, **P(unpaired t-test)<0.001.* (K) Mean number of pH3+ cells, a mitotic
724 marker. Data points denote mean ± s.e.m, n = 10. Scale bar - 10 μm. See also Figure
725 S2.

726

727 **Figure 3. ROS imbalance in CySCs promotes differentiation of both GSCs and**
728 **CySCs**

729 (A-D) Number of early CySCs (Zfh1^{+}) (A'- B'), late differentiating CCs (Eya^{+}) (A - B)
730 and Zfh1, Eya co-expressing population (A''- B'') were imaged, represented
731 schematically (C) and quantified with respect to control and *Sod1RNAi* lines (D). Data
732 points represent mean ± s.e.m, n = 10, ****P(unpaired t-test)<0.0001*. (E-F) The effect
733 of Sod1 depletion in CySCs on the differentiation status of GSCs as observed using
734 *Bam-GFP* reporter line. (G) The relative distance of the differentiation initiation zone
735 (Bam^{+}) from the hub (red) in control and *Sod1i* testis quantified in single sections and
736 shown as mean ± s.e.m, n = 10, ****P(unpaired t-test)<0.0001.* (H-J) The shape and
737 size of the spectrosomes marked with α-spectrin (green) were imaged (I''-J'') and
738 quantified for their distance from the hub (marked with asterisk) (H), n = 10,
739 ****P(unpaired t-test)<0.0001*. Branched fusome marks differentiating populations (I'-
740 J'). (K-L) Represents the rosette arrangement of Vasa^{+} GSCs flanking the hub. The
741 digitally magnified region around the hub (dotted line) as seen in control (K#) and
742 *Sod1RNAi* (L#). (M-N) Comparative staining of CySC-GSC contacts through adherens
743 junction using E-cadherin (monochrome/green). Dotted area near the hub has been
744 expanded as inset to show loss of E-cadherin network. (O) E-cadherin intensity
745 histogram plot generated from ImageJ representing the mean intensity of expression
746 in the region flanking the hub and GSCs. (P-Q) Fold change in expression of Stat
747 dependent transcripts Socs36E (P) and Ptp61F (Q) among control and *Sod1i* niche,
748 obtained through qPCR. Data is shown as mean ± s.e.m, n = 3, ****P(unpaired t-*
749 *test)<0.0001*. ns – not significant. Scale bar - 10 μm. See also Figure S3.

750

751 **Figure 4. Altered CySC redox state affects niche maintenance signals.**

752 (A-B) The expression of cell polarity marker Dlg (red) in control and *Sod1i* stem-cell
753 niche (A''-B''), (C-D) Representative image showing pErk distribution parallelly with Tj^+
754 cells and its expression pattern through Fire LUT (C''-D''). Scale bar - 10 µm. Mean
755 florescence intensity (MFI) corresponding to Dlg level (E) was quantified, n = 75,
756 ****P(unpaired t-test)<0.0001.* (F) MFI of total pErk expression was quantified, n =200,
757 ****P(unpaired t-test)<0.0001*. (G'-H') Representative image showing distribution of
758 Patched (Ptc) in Tj^+ cells in control and *Tj>Sod1i*. (I-J) Quantification of Ptc (I) and Hh
759 effector Ci (J) expression through fluorescence intensity as mean ± s.e.m, n (Ptc) =
760 90, n (Ci) = 200, ****P(unpaired t-test)<0.0001* (K-L) The number of $Vasa^+$ (K) and Tj^+
761 (L) cells across control, *Sod1i*, and *Sod1i/Hhi* rescue samples depicted as mean ±
762 s.e.m, n = 10, ****P(unpaired t-test)<0.0001*. See also Figure S4.

763

764 **Figure 5. Low CySC ROS sustains GSC maintenance**

765 (A-B) Bar graphs illustrating variations in $Vasa^+$ GSC (A) and Tj^+ CySCs (B) numbers
766 upon overexpressing Sod1 (*Tj>Sod*^{OE}), represented as mean ± s.e.m, n = 10,
767 ****P(unpaired t-test)<0.0001, *P(unpaired t-test)<0.01*. (C-E) The spectrosomes
768 labelled with α-spectrin (α-spec) were imaged (C'-D') and their number was quantified
769 (E), n = 10, ***P(unpaired t-test)<0.001*. (F-H) The initiation of gonialblast differentiation
770 was determined by measuring the distance of Bam^+ zone from hub (red), n = 10,
771 **P(unpaired t-test)<0.01* (F), (G''-H'') shows distribution of Bam^+ reporter expressing
772 cells. Scale bar - 10 µm. See also Figure S5.

773

774 **Figure 6. Proposed role of intercellular redox balance in germline maintenance**
775 **and differentiation**

776 GSC and CySC are associated with different mitochondria abundance which
777 correspond to the presence of a redox differential between two stem cell populations.
778 Disequilibrated redox potential among the two populations due to depletion of
779 Superoxide dismutase, enhances CySC proliferation and precocious GSC
780 differentiation, thereby disrupting the homeostatic balance between the two stem
781 populations.

Figure 1

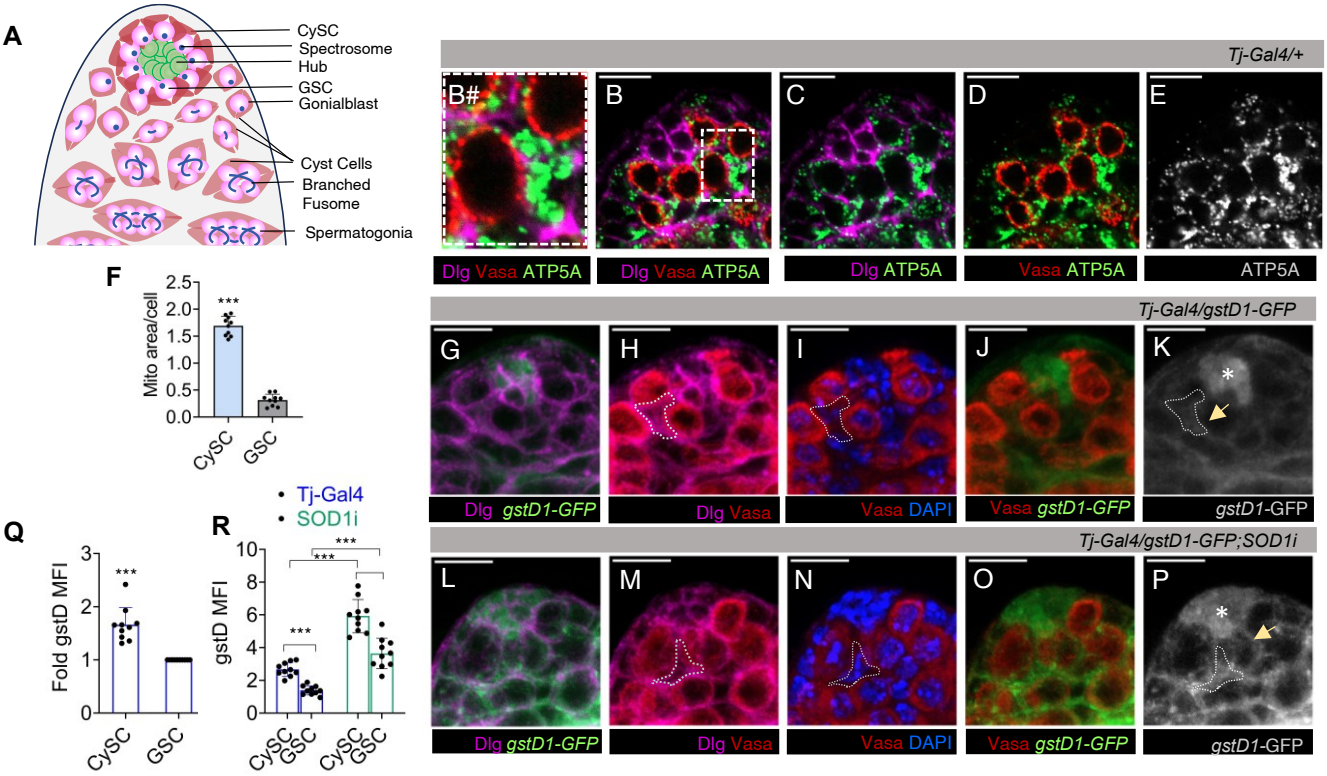
A
CySC
Spectrosome
Hub
GSC
Gonialblast
Cyst Cells
Branched Fusome
Spermatogonia
Tj-Gal4/+
B#
B
C
D
E
Dlg Vasa ATP5A
Dlg Vasa ATP5A
Dlg ATP5A
Vasa ATP5A
ATP5A
F
Mito area/cell
2.5
2.0
1.5
1.0
0.5
0.0
***
CySC
GSC
Tj-Gal4/gstD1-GFP
G
H
I
J
K
Dlg gstD1-GFP
Dlg Vasa
Vasa DAPI
Vasa gstD1-GFP
gstD1-GFP
Tj-Gal4/gstD1-GFP;SOD1i
L
M
N
O
P
Dlg gstD1-GFP
Dlg Vasa
Vasa DAPI
Vasa gstD1-GFP
gstD1-GFP
Q
Fold gstD MFI
3
2
1
0
***
CySC
GSC
R
Tj-Gal4
SOD1i
gstD MFI
10
8
6
4
2
0
***
***
***
CySC
GSC
CySC
GSC

Figure 2

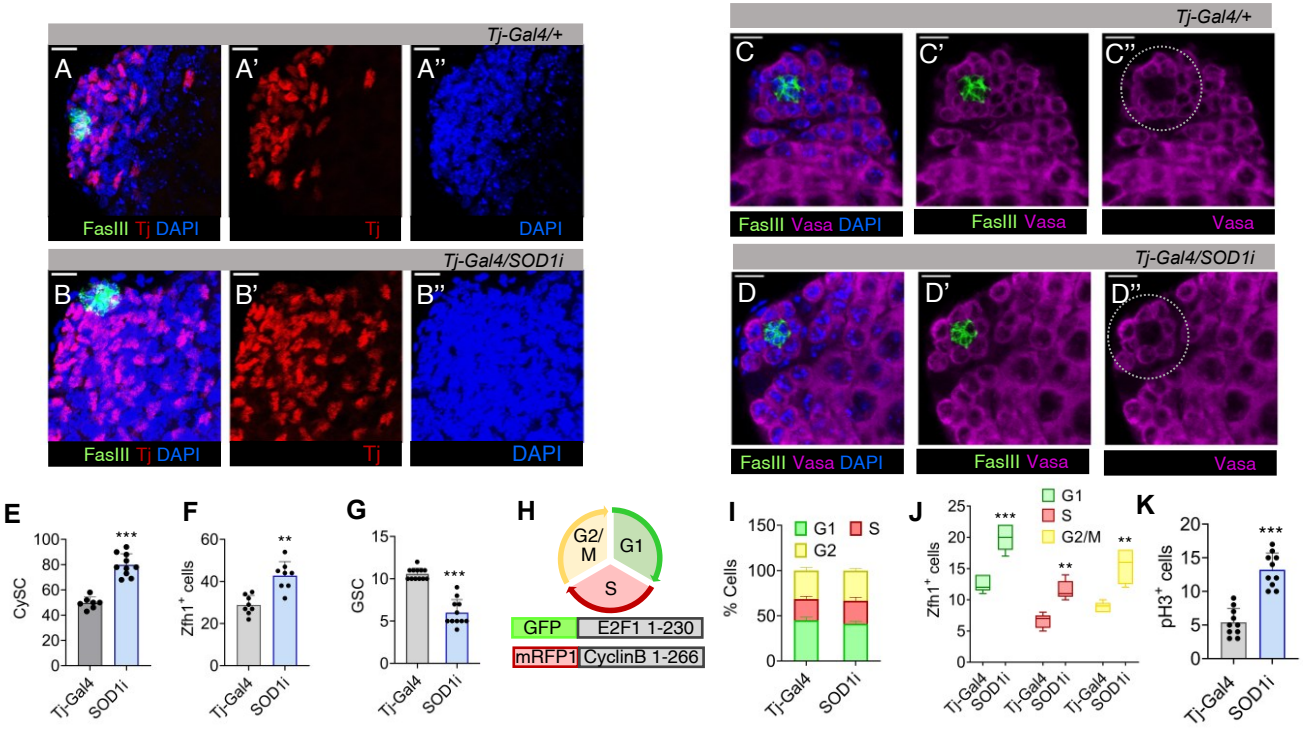
Tj-Gal4/+
A
A'
A''
FasIII Tj DAPI
Tj
DAPI
Tj-Gal4/SOD1i
B
B'
B''
FasIII Tj DAPI
Tj
DAPI
Tj-Gal4/+
C
C'
C''
FasIII Vasa DAPI
FasIII Vasa
Vasa
Tj-Gal4/SOD1i
D
D'
D''
FasIII Vasa DAPI
FasIII Vasa
Vasa
E
CySC
Tj-Gal4
SOD1i
F
Zfh1+ cells
G
GSC
H
G2/M
G1
S
GFP
E2F1 1-230
mRFP1
CyclinB 1-266
I
% Cells
G1
S
G2
J
Zfh1+ cells
G1
S
G2/M
K
pH3+ cells

Figure 3

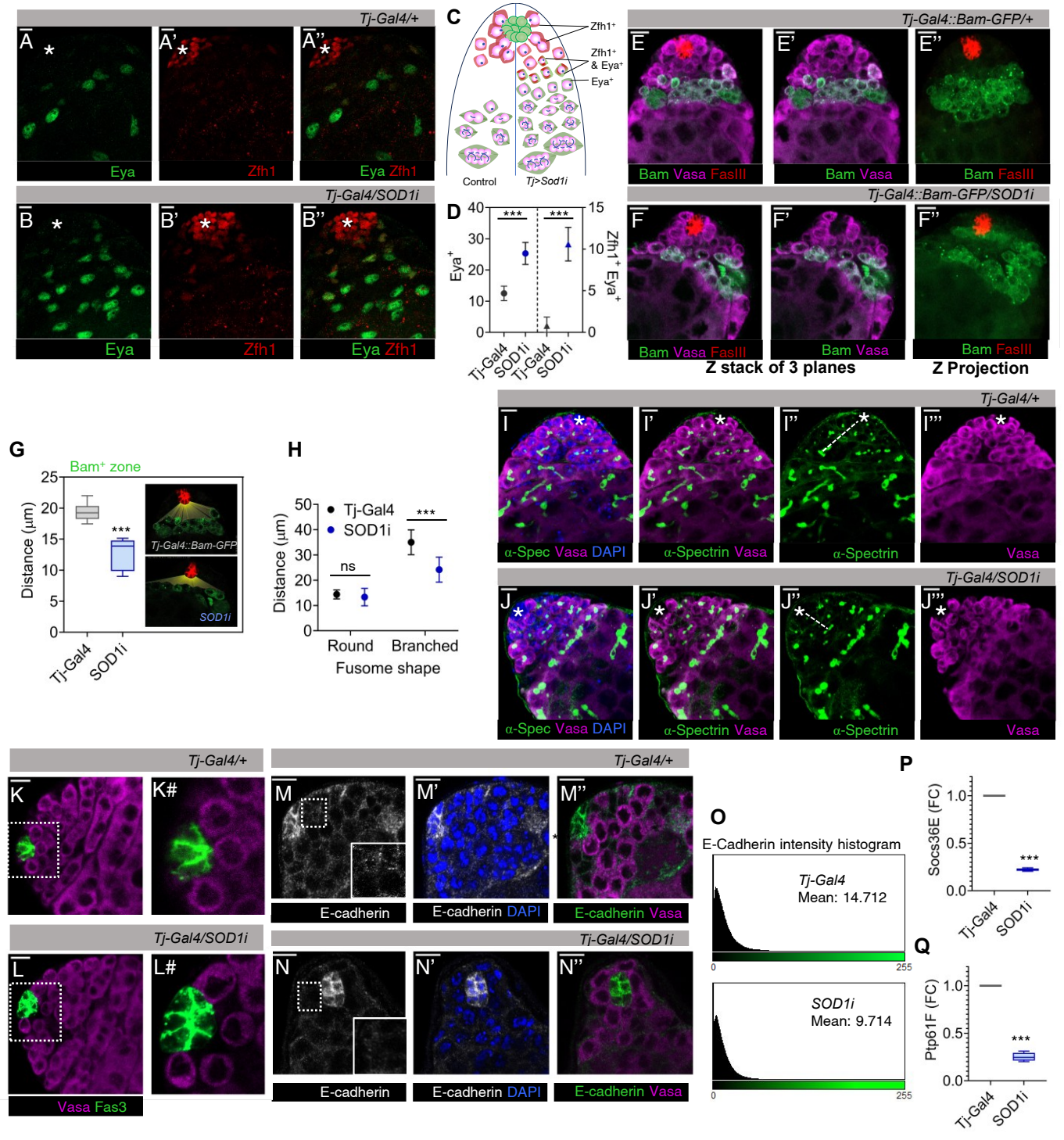
Tj-Gal4/+
A
A'
A''
Eya
Zfh1
Eya Zfh1
Tj-Gal4/SOD1i
B
B'
B''
Eya
Zfh1
Eya Zfh1
C
Zfh1+
Zfh1+ & Eya+
Eya+
Control
Tj>Sod1i
D
Eya+
Zfh1+ Eya+
***
***
Tj-Gal4
SOD1i
Tj-Gal4
SOD1i
Tj-Gal4::Bam-GFP/+
E
E'
E''
Bam Vasa FasIII
Bam Vasa
Bam FasIII
Tj-Gal4::Bam-GFP/SOD1i
F
F'
F''
Bam Vasa FasIII
Bam Vasa
Bam FasIII
Z stack of 3 planes
Z Projection
G
Bam+ zone
Distance (µm)
***
Tj-Gal4::Bam-GFP
SOD1i
Tj-Gal4
SOD1i
H
Tj-Gal4
SOD1i
Distance (µm)
ns
***
Round
Branched
Fusome shape
Tj-Gal4/+
I
I'
I''
I'''
α-Spec Vasa DAPI
α-Spectrin Vasa
α-Spectrin
Vasa
Tj-Gal4/SOD1i
J
J'
J''
J'''
α-Spec Vasa DAPI
α-Spectrin Vasa
α-Spectrin
Vasa
Tj-Gal4/+
K
K#
Tj-Gal4/SOD1i
L
L#
Vasa Fas3
Tj-Gal4/+
M
M'
M''
E-cadherin
E-cadherin DAPI
E-cadherin Vasa
Tj-Gal4/SOD1i
N
N'
N''
E-cadherin
E-cadherin DAPI
E-cadherin Vasa
O
E-Cadherin intensity histogram
Tj-Gal4
Mean: 14.712
SOD1i
Mean: 9.714
0
255
P
Socs36E (FC)
***
Tj-Gal4
SOD1i
Q
Ptp61F (FC)
***
Tj-Gal4
SOD1i

Figure 4

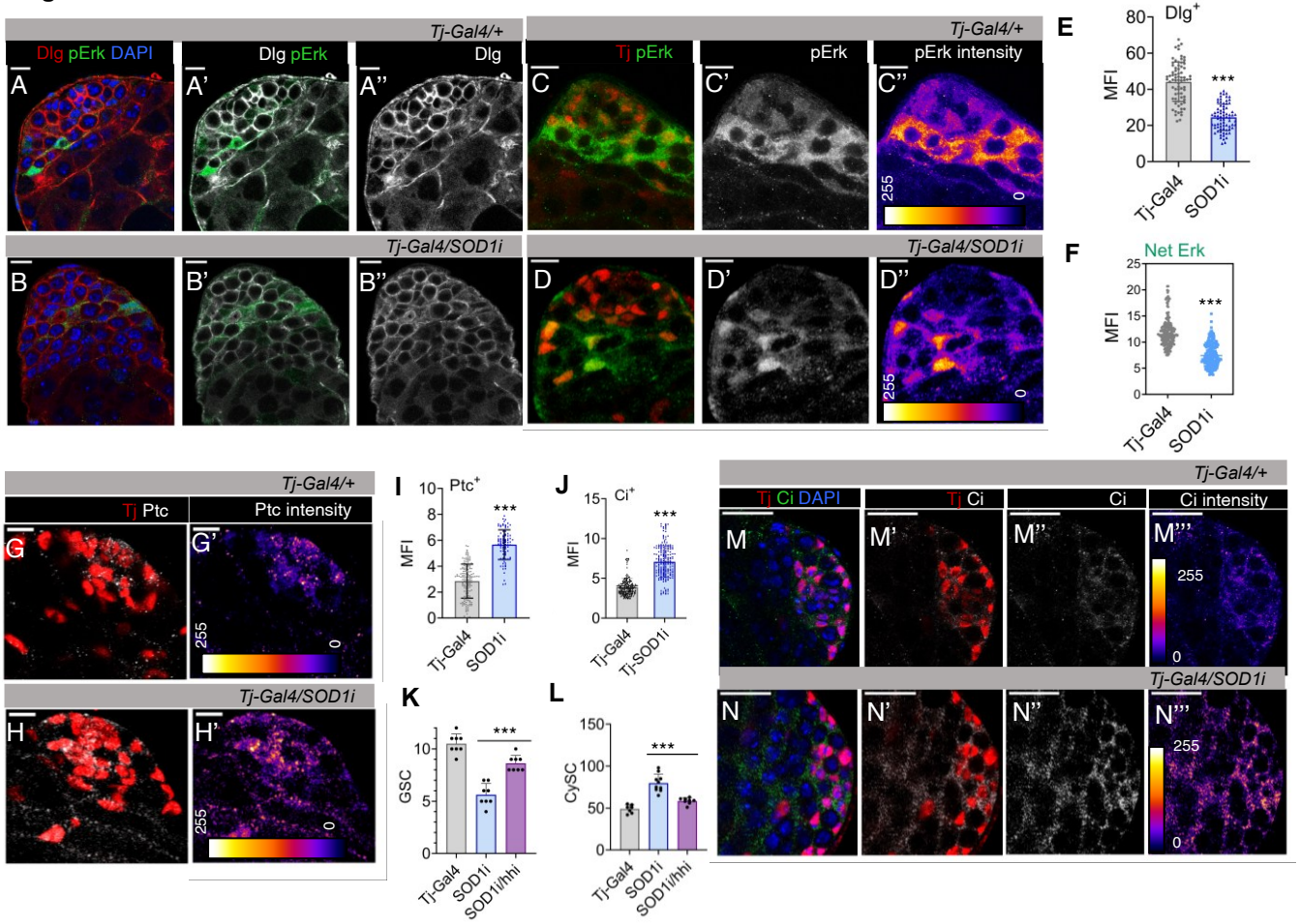
Tj-Gal4/+
Dlg pErk DAPI
Dlg pErk
Dlg
Tj pErk
pErk
pErk intensity
A
A'
A''
C
C'
C''
255
0
Tj-Gal4/SOD1i
B
B'
B''
D
D'
D''
E
Dlg+
MFI
***
Tj-Gal4
SOD1i
F
Net Erk
G
G'
Tj Ptc
Ptc intensity
H
H'
I
Ptc+
J
Ci+
K
GSC
SOD1i/hhi
L
CySC
Tj Ci DAPI
Tj Ci
Ci
Ci intensity
M
M'
M''
M'''
N
N'
N''
N'''

Figure 5

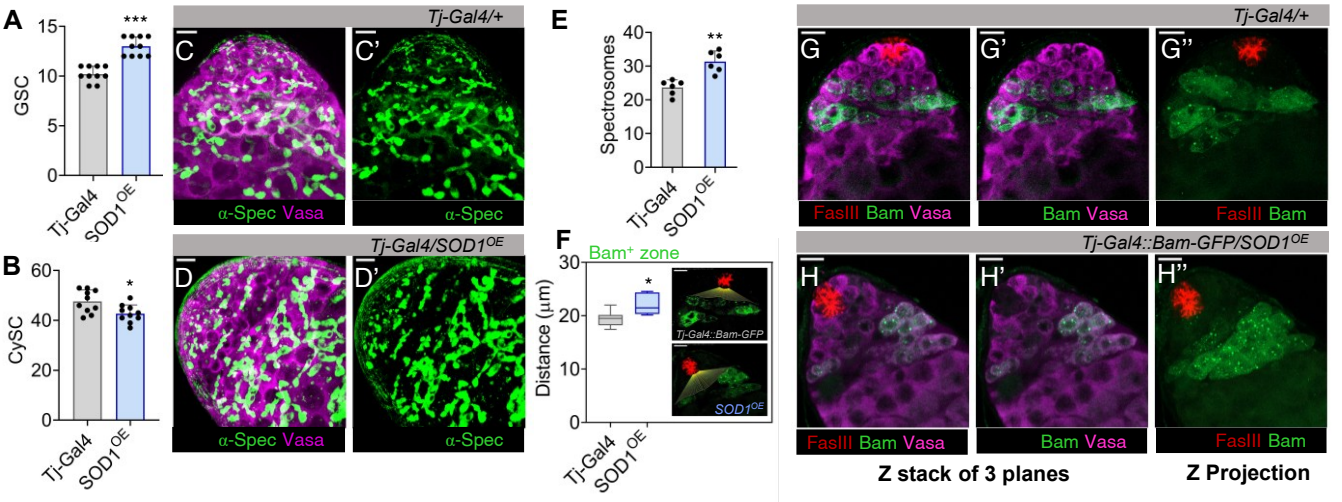
A
GSC
15
10
5
0
***
Tj-Gal4
SOD1OE
B
CySC
60
40
20
0
*
Tj-Gal4
SOD1OE
Tj-Gal4/+
C
C'
α-Spec Vasa
α-Spec
Tj-Gal4/SOD1OE
D
D'
α-Spec Vasa
α-Spec
E
Spectrosomes
40
30
20
10
0
**
Tj-Gal4
SOD1OE
F
Bam+ zone
Distance (μm)
30
20
10
0
*
Tj-Gal4
SOD1OE
Tj-Gal4::Bam-GFP
SOD1OE
Tj-Gal4/+
G
G'
G''
FasIII Bam Vasa
Bam Vasa
FasIII Bam
Tj-Gal4::Bam-GFP/SOD1OE
H
H'
H''
FasIII Bam Vasa
Bam Vasa
FasIII Bam
Z stack of 3 planes
Z Projection

Figure 6

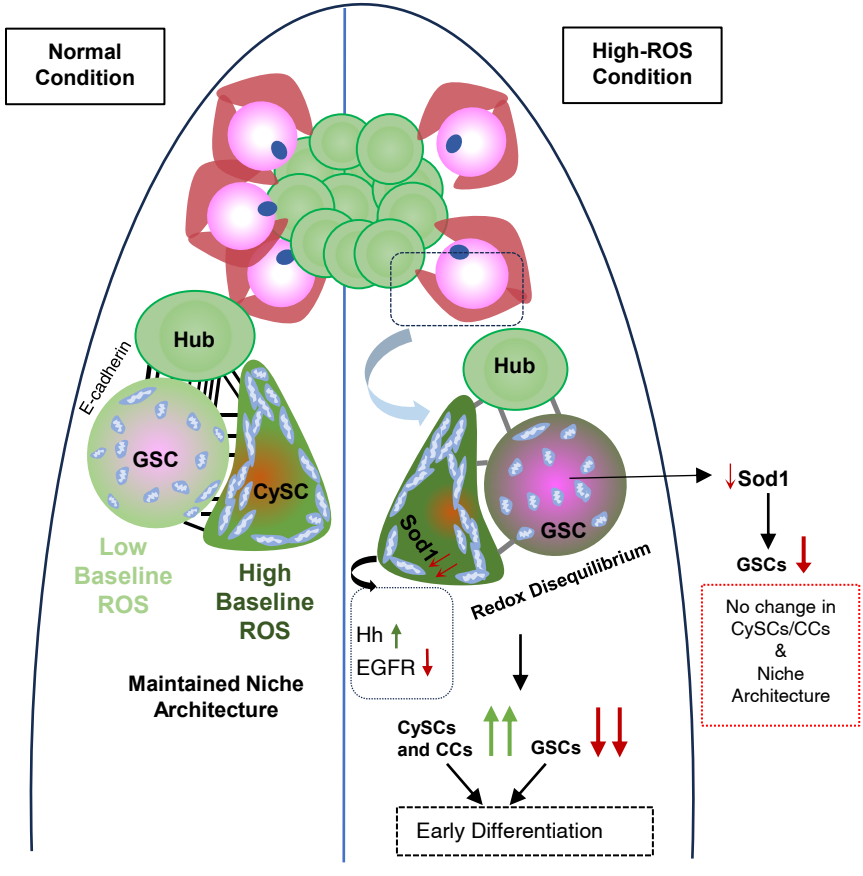
Normal Condition
High-ROS Condition
Hub
E-cadherin
GSC
CySC
Low Baseline ROS
High Baseline ROS
Maintained Niche Architecture
Hub
Sod1
GSC
Redox Disequilibrium
Hh
EGFR
CySCs and CCs
GSCs
Early Differentiation
Sod1
GSCs
No change in CySCs/CCs & Niche Architecture